



## OPEN ACCESS

## EDITED BY

Yang Li,  
Anhui University of Science and  
Technology, China

## REVIEWED BY

Umar Daraz,  
Lanzhou University, China  
Yuying Liu,  
Sichuan Agricultural University, China

## \*CORRESPONDENCE

Shili Guo,  
✉ guoshili@swufe.edu.cn

## SPECIALTY SECTION

This article was submitted to  
Biogeochemical Dynamics,  
a section of the journal  
Frontiers in Environmental Science

RECEIVED 14 February 2023

ACCEPTED 02 March 2023

PUBLISHED 16 March 2023

## CITATION

Li C, Guo S, Shang S, Qi P and Li B (2023),  
Structure and biogeochemical process of  
microaggregates in a water source area  
of China's South-to-North Water  
Diversion Project according to different  
land use types.  
*Front. Environ. Sci.* 11:1165454.  
doi: 10.3389/fenvs.2023.1165454

## COPYRIGHT

© 2023 Li, Guo, Shang, Qi and Li. This is an  
open-access article distributed under the  
terms of the [Creative Commons  
Attribution License \(CC BY\)](#). The use,  
distribution or reproduction in other  
forums is permitted, provided the original  
author(s) and the copyright owner(s) are  
credited and that the original publication  
in this journal is cited, in accordance with  
accepted academic practice. No use,  
distribution or reproduction is permitted  
which does not comply with these terms.

# Structure and biogeochemical process of microaggregates in a water source area of China's South-to-North Water Diversion Project according to different land use types

Chunjie Li<sup>1</sup>, Shili Guo<sup>2\*</sup>, Songhao Shang<sup>3</sup>, Pengcheng Qi<sup>1</sup> and Bailian Li<sup>4</sup>

<sup>1</sup>School of Geography and Tourism, Nanyang Normal University, Nanyang, China, <sup>2</sup>School of Economics, Southwestern University of Finance and Economics, Chengdu, China, <sup>3</sup>State Key Laboratory of Hydrosience and Engineering, Tsinghua University, Beijing, China, <sup>4</sup>Department of Botany and Plant Sciences, Ecological Complexity and Modeling Laboratory, University of California, Riverside, Riverside, CA, United States

Soil biogeochemical processes have the potential to impact water quality in source areas of water diversion projects. This study aimed to explore the differences in biochemical processes and mechanisms at the microaggregate scale for different land use types in the water source area of China's Middle Route of the South-to-North Water Diversion Project. The study compared four typical land use types—forests, shrublands, terraces, and cultivated land—by characterizing the microaggregates using various analytical techniques, including scanning electron microscopy (SEM), SEM-EDS plane scan analysis, X-ray diffraction (XRD), X-ray fluorescence (XRF) spectroscopy, and Fourier transform infrared (FTIR) spectroscopy. Microaggregates from forests and shrublands had a flocculent spatial structure, while those from terraces had a nondirectional plate-like spatial structure, and those from cultivated land had a laminar spatial structure. Additionally, elements such as Mg, Al, and Fe were enriched in clay particles when combined with microaggregates. The mineral composition of clay varied significantly between different land use practices, with illite, chlorite, anorthite, albite, and quartz present in higher proportions in terraces and cultivated land than in forests and shrublands. Moreover, the contents of transitional elements such as Ti, Fe, Zn, Y, and Zr increased with each successive land use practice. Soil organic matter (SOM) was observed to decline in the order of forest > shrubland > terraces > cultivated land. Over-tillage appeared to be the primary mechanism of organic matter loss due to long-term tillage. The results of this study provide valuable insights into soil erosion and chemical transport dynamics. The mineral composition and spatial structure of microaggregates are important determinants of soil biochemical processes and mechanisms, which can influence water quality. The findings suggest that forest and shrubland management practices may be more conducive to maintaining soil health and water quality in source areas of water diversion projects.

## KEYWORDS

Water source area, Microaggregates, Scanning electron microscopy, X-Ray Diffraction, Fourier transform infrared

## 1 Introduction

Soils are the most heterogeneous part of the biosphere and have extremely variable properties and processes from the nanoscale to the macroscale (Kuzyakov and Blagodatskaya, 2015). As the basic unit of the soil structure, soil aggregates are involved in many processes, such as hydrology, soil erosion, soil microbial dynamics, and biogeochemical cycles (Cerdà, 1996; Sander et al., 2008; Kong et al., 2011; Pronk et al., 2012; Lehmann and Kleber, 2015). Soil aggregates also involve water and solute movement, gas exchange, soil organic matter (SOM), nutrient dynamics, and root infiltration (Rabot et al., 2018). Aggregates form the material basis of a good soil structure and are the main carriers of nutrients, such as soil organic carbon (SOC), N, P, and K. The content and composition of soil aggregates are closely interrelated with soil fertility and erosion resistance and exert significant influences on numerous physical, chemical, and biological properties of soil. Short-term evolution in soil clay minerals caused by changes in the nutrient balance and physicochemical properties in soils from different land use types has been demonstrated (Liu et al., 2017). Different land use practices can influence the soil environment and agglomerate evolutionary processes *via* vegetation types and anthropogenic interventions that influence soil surface litter content, microbial abundance, etc.

Changes in the land use type can affect the biogeochemical characteristics of soils, such as their texture and microbial communities, and their biochemical transformation of nutrients (Mganga et al., 2016). Aggregates profoundly affect soil fertility and soil erosion resistance (Lu et al., 2016) and are key to increasing soil infiltration and aeration and reducing soil erosion and runoff (Haydu-Houdeshell et al., 2018). The water source area of the Middle Route of the South-to-North Water Diversion Project in China is an environmentally sensitive and ecologically fragile zone, which is located in the subtropical warm temperate transition zone in the hinterland of East Asia. The land use types in this water source area are complex and diverse, and soil erosion is serious (Li and Guo, 2022). Soil degradation and non-point-source pollution caused by land use have attracted widespread attention in this area. In the near future, sediment deposition and water quality safety will become one of the main challenges in reservoir management (Collins et al., 2011; McCrackin et al., 2016; Tang et al., 2019). In recent years, the physicochemical properties of soils in water source areas have been studied (Li and Guo, 2022); however, systematic research on the structure and biochemical properties of microaggregates in different land use types in key water areas of the world remains lacking. Study of the function of biogeochemical interfaces at microaggregate mineral surfaces requires the simultaneous consideration of chemical, physical, and biological factors (Witzgall et al., 2021). The micro-characteristics of soil aggregates can be expressed through the macroscopic phenomena of soils, and macro-behaviors such as land use may affect the micro-characteristics of soil aggregates. The land use type may have an effect on the process of soil

development, which may be accompanied by the soil aggregate structure and biogeochemical processes at the soil micro-level. This paper attempts to prove whether changes in land use types will affect the process of soil development *via* the micro-processes of soil aggregates. We sought to demonstrate the differences in biochemical processes and their mechanisms at the microagglomerate scale for different land use types in a water source area of the South-to-North Water Diversion Project. This is of great importance for understanding the structure, composition, and incubation environment of aggregates and nanoscale biogeochemical cycling processes in this region.

## 2 Materials and methods

### 2.1 Overview of the study area

The study area was located at the Middle Route of the South-to-North Water Diversion Project in China, which is in the transition zone between China's northern and southern climates (Li and Guo, 2022). The Danjiangkou Reservoir is a water source area at the Middle Route of the South-to-North Water Diversion Project in China (Figure 1), which is one of the largest water diversion projects in the world (Li et al., 2015). The region is located in a westerly wind zone with an average annual temperature of 15.8°C. The average annual precipitation ranges from 900 to 1100 mm. The geological type of the study area is limestone marine strata. Karst rocky desertified landscapes are widely distributed in this region (Figure 1). The landform type is predominantly mountainous and hilly. Soil-forming parent material is developed from limestone and gneiss, with a loose texture. The soil types are predominantly yellow-brown soil and sandy-ginger black soil. The soil is relatively barren, and the terrain is mainly sloping, making it vulnerable to water erosion. The average soil erosion modulus is about 3517 t km<sup>-2</sup> a<sup>-1</sup>. The main land use types in the study area include forests, shrublands, terraces, and cultivated land (Figure 1).

### 2.2 Collection and processing of soil samples

We selected four typical land use types, including forests, shrublands, terraces, and cultivated land, with five parallel sampling sites for each type of land use. We collected undisturbed soil samples from the top 10 cm of soil. Dead leaves were removed from the topsoil prior to sampling, and five soil samples were collected within 10 × 10 m quadrats for each land use type using the five-point sampling method in September 2020. Approximately 500 g of the mixed samples were randomly taken and brought to the Soil and Environment Laboratory at Nanyang Normal University for analysis. The samples were first frozen at -80°C for 1 h and then placed in a freeze dryer and dried at low temperature under vacuum (vacuum, 0.05 MPa, temperature, 50°C, 24 h). Then, the plant roots and litter were removed, and the

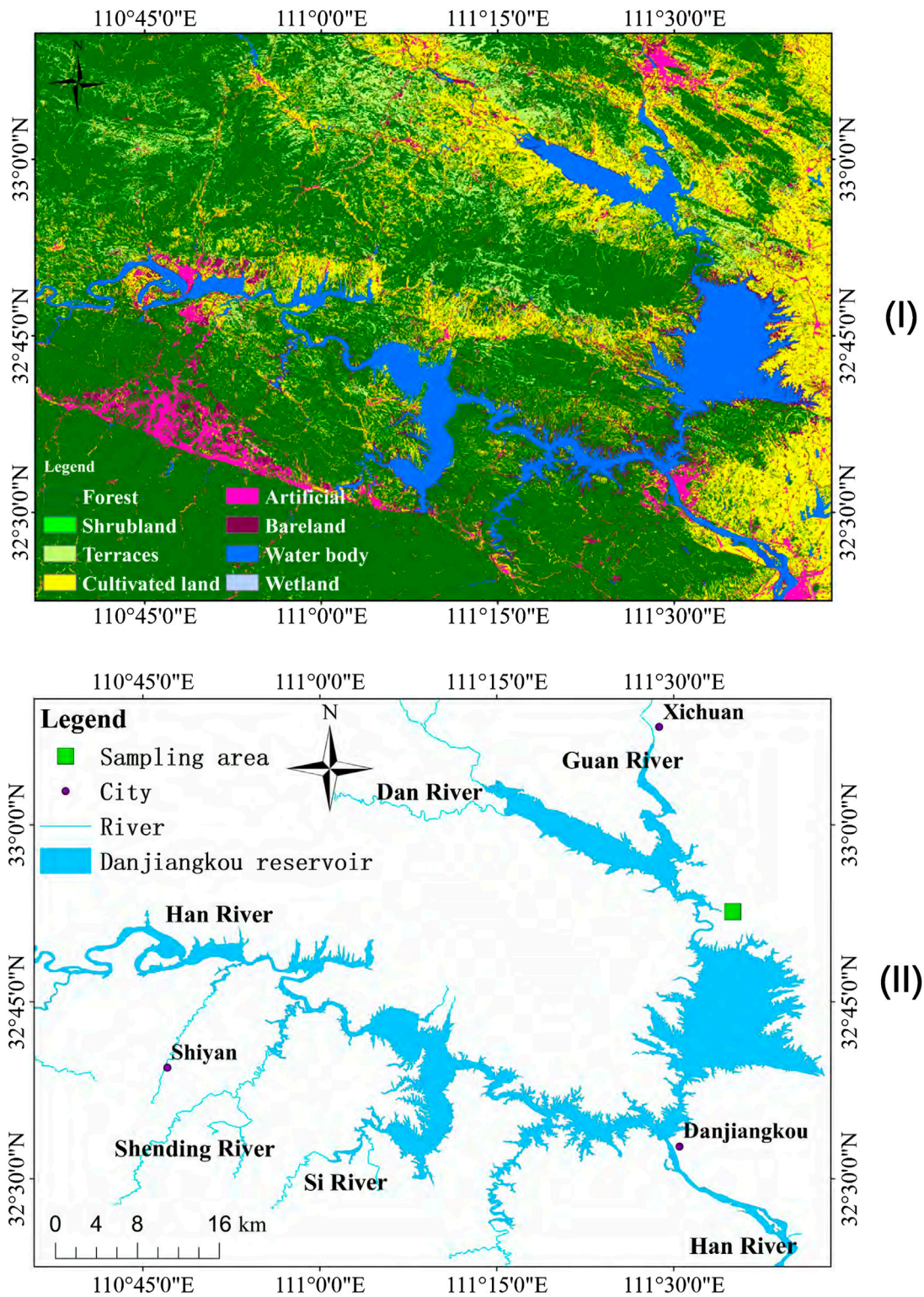


**FIGURE 1**  
Map (I) shows the land use types in the study area, and map (II) shows the location of the research region in the Danjiangkou Reservoir of China.

coarse particles were removed from the soil by passing it through a 2-mm sieve. Subsequently, the particle size distribution of soil microagglomerates observed by SEM was analyzed using Nano Measurer 1.2 software.

### 2.3 SEM-EDS analysis of soil samples

SEM (Zeiss EVO 18, Zeiss, Germany) was used to study the microaggregate structure and the planar distribution of key

elements. Aggregates were glued to a conductive adhesive and observed after gold spraying using an ion sputterer (Ersoy et al., 2008). SEM-EDS plane scan analysis was performed by energy dispersive spectroscopy (EDS; Bruker Nano, Berlin, Germany, XFlash 6|30) at an acceleration voltage of 10 kV. The main elements characterized by SEM-EDS were C, O, Si, Al, Fe, Ca, Mg, and P. For X-ray energy spectrometry analysis, the electron beam was accelerated to 10 kV, the beam current was 0.2 nA, the working distance was 80 mm, and the X-ray emission angle was 35°; 4,096 signals were recorded. The recording time was 40 s, and the thickness of detection was 0.45 mm. SEM-EDS plane scan analysis was used to analyze the elemental compositions and distributions in different regions of the microaggregates. The planar distribution of the elements in the detection area was obtained by scanning the detection area.

## 2.4 Mineral analysis of soil samples

In the pre-treatment, the SOC was removed with H<sub>2</sub>O<sub>2</sub> (30%, analytical purity) to disperse the soil particles. The samples were then dried and finally ground with an agate mortar until they were very fine particles. The samples were collected through a 400-mesh sieve and analyzed for mineral composition by X-ray diffraction. Soil minerals were analyzed using the X-ray diffraction technique. The treated samples were made into powder wafers and analyzed by XRD using an X-ray diffractometer (Rigaku SmartLab 9kW Full Auto X-ray Diffractometer). The measurement conditions were as follows: Cu-K $\alpha$  target, graphite monochromator filter, tube voltage was 40 kV, current was 150 mA, the scan range was 5°–80° (2 $\theta$ ), scan speed was 6° min<sup>-1</sup> (2 $\theta$ ), and the step size was 0.02°. The diffraction peaks obtained from the X-ray diffraction analysis were processed using Jade software, and the results were compared with standard PDF cards. The clay mineral types were identified using the clay mineral analysis method. The total clay and non-clay mineral contents were calculated directly by measuring the integrated intensities of selected diffraction peaks of clay and non-clay minerals in the diffraction patterns according to the adiabatic method and were calculated as follows:

$$X_i = \left[ \frac{I_i}{K_i} / \left( \sum \frac{I_i}{K_i} \right) \right] \times 100\%$$

where  $X_i$  is the content of mineral  $i$  (%),  $K_i$  is the reference intensity of mineral  $i$ , and  $I_i$  is the intensity of a diffraction peak of mineral  $i$ .

## 2.5 X-ray fluorescence spectroscopy

The dried soil samples were ground to pass through a 200-mesh sieve, weighed, and pressed into thin slices, and then placed into an X-ray fluorescence spectrometer for elemental analysis (AXIOS W4400, PANalytical B.V., Almelo, Netherlands). The requirements were as follows: maximum power was 4.0 kW, maximum excitation voltage was 60 kV, maximum current was 125 mA, SST ultra-sharp ceramic end window (75  $\mu$ m), Rh target X-ray tube, and a 68-position (32 mm diameter) sample changer. The results were calibrated using SuperQ 4.0 quantitative analysis

software. The software automatically performed spectral intensity calculations, Compton scattered-ray internal standard corrections, interfering spectral line corrections, and matrix corrections.

## 2.6 Fourier transform infrared spectroscopy

The rapid development of FTIR has provided an efficient means of characterizing the structure and composition of organic micro-molecules in soils. Numerous studies have shown that FTIR has significant advantages in characterizing the organic environment of soils (Margenot et al., 2015). For our analysis, dried soil samples were randomly sampled individually, stones and grass roots were picked out, and the soil was passed through a 0.149-mm soil sieve. The samples were then mixed with dried potassium bromide (spectroscopical purity) at a mass ratio of 1:90 and ground rapidly and thoroughly by hand with an agate mortar and pestle under an infrared lamp. The tablets were compacted with a press at 10 kPa and placed in a Thermo Nicolet iS5 FTIR spectrometer (Thermo Fisher Scientific, United States) for measurement (Li et al., 2022). The background value of KBr was used, and the spectra were acquired in the range of 400–4000 cm<sup>-1</sup> at a resolution of 4 cm<sup>-1</sup>. Some 32 scans were taken, and each sample was scanned five times. The similarities were compared and averaged, and sample IR spectra were obtained after subtracting the background values. The acquired spectral data underwent preprocessing using Thermo Scientific OMNIC 6.0 software. This involved application of a calibration function to remove baseline effects, followed by standard normalization to correct for differences in sample weighing. Subsequently, the software application was utilized to calculate the integral of the relative peak area of the main peaks of the FTIR spectrum.

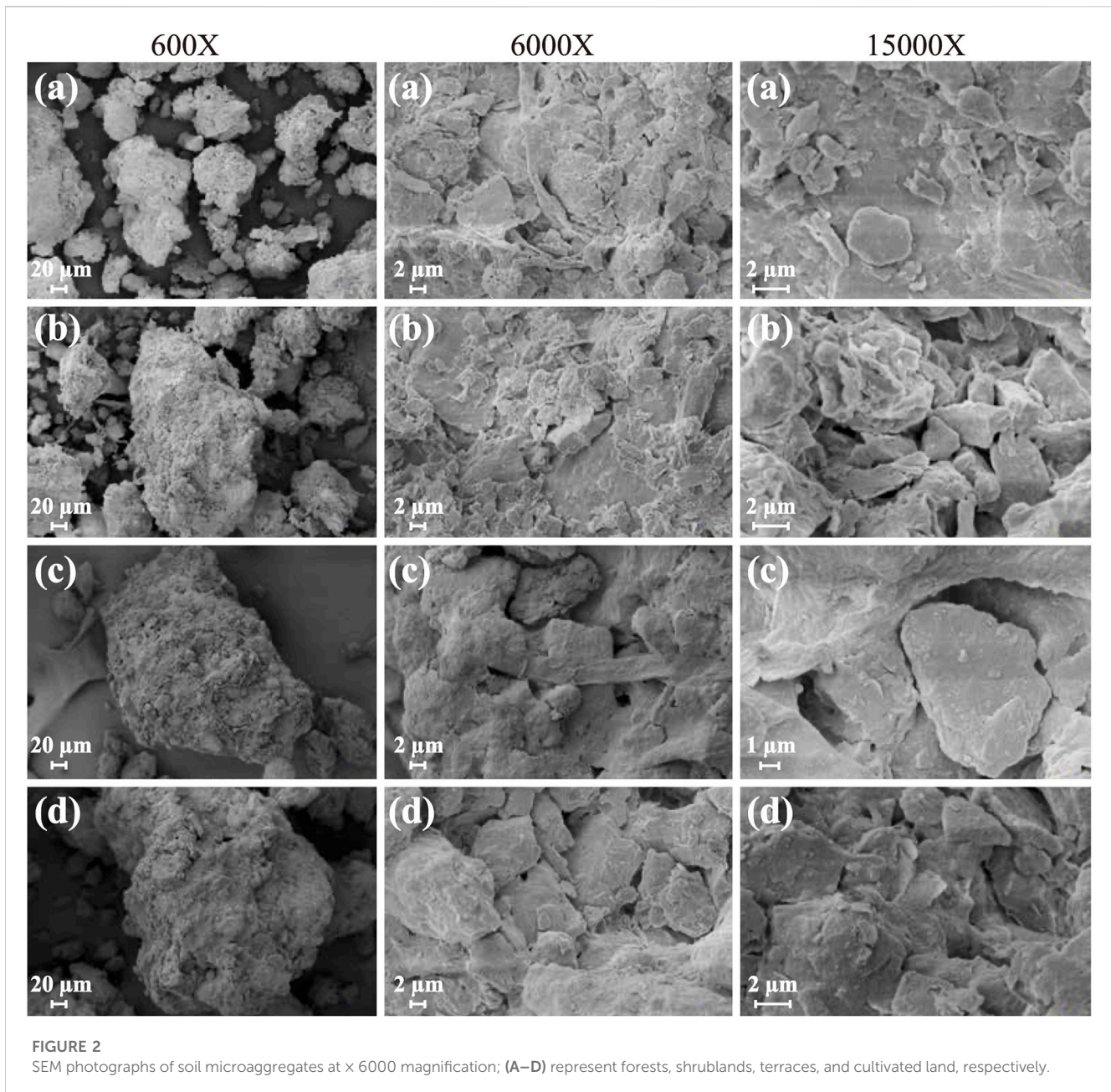
## 2.7 Data statistics and graphing

Statistical analyses were performed using SPSS 15.0 for Windows (SPSS Inc., Chicago, IL). A map was generated using ArcGIS 10.0 (ESRI, Redlands, CA, United States; <http://www.esri.com/software/arcgis>). All connecting lines were generated using Origin 8.1 software (Origin Lab Corp., v 8.1). Sentinel-2 satellite data were used for the LULC classifications, which were made freely accessible by the European Space Agency (ESA). Satellite data analysis was performed using ENVI 5.3.1 and ArcGIS 10.0 software applications.

# 3 Results and discussion

## 3.1 Microaggregate structure under different land use types

Aggregates, consisting of mineral and organic particles bonded together by soil processes, are the fundamental structural units of soils (Parent et al., 2012). They play a role in a variety of structural, physicochemical, and biological processes, influencing water and nutrient movement, as well as their availability to plants (Six et al., 2004; Bronick and Lal, 2005). Additionally, the structure of these



aggregates also affects ecosystem characteristics, such as water retention, soil water movement, erosion, nutrient cycling, root penetration, and crop yield (Bronick and Lal, 2005). Over time, soil morphology, composition, and mineralogical properties can be altered due to ongoing development (Igwe et al., 2005). The SEM results show that the structure of microaggregates varies significantly between land use types. The numbers of clay particles on the surfaces of microaggregates from forests and shrublands were high, and the microaggregates showed a flocculent spatial structure (Figures 2, 3). By contrast, the numbers of clay particles on the surfaces of microaggregates from terraces and cultivated land were relatively low. The microaggregates from terraces showed a non-directional plate spatial structure, while those from cultivated land showed a laminar spatial structure. Nanoporous structures were seen in

soils from forests, shrublands, terraces, and cultivated land, and remnants of plant roots and litter were found. Litter-derived SOC has been proven to be incorporated into aggregate structures (Witzgall et al., 2021). Forests and shrublands are relatively high in carbonate minerals and have a relatively loose microaggregate spatial structure compared to terraces and cultivated land (Table 1; Figures 2, 3). Microaggregates may have formed initially through the gradual incorporation of clays, SOC, and cations during physicochemical reactions (Oades and Waters, 1991; Duiker, 2003). The complex interactions between aggregates can be synergistic or destructive (Bronick and Lal, 2005). In some cases, microaggregates are also the turnover products of large aggregates. The spatial structures of microaggregates from terraces and cultivated land are relatively dense. The microaggregate structure is affected by frequent compaction from farm implements during

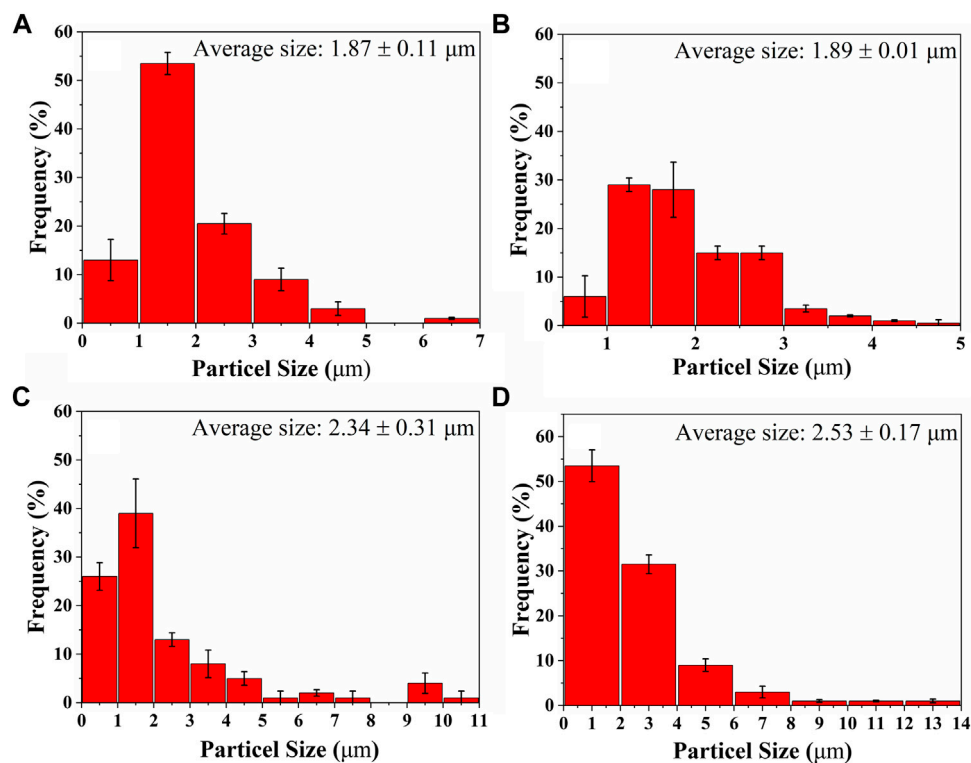


**FIGURE 3**  
Frequency of particle size distribution of soil microaggregates.

**TABLE 1** Mass fraction of soil minerals using XRD with standard deviation (%).

Mineral	Forest	Shrubland	Terrace	Cultivated land
Dolomite	57.01 ± 4.74	44.41 ± 3.01	3.70 ± 0.59	4.84 ± 0.69
Calcite	2.88 ± 0.35	4.14 ± 0.56	1.12 ± 0.15	1.20 ± 0.15
Chlorite	0.83 ± 0.18	2.74 ± 0.50	6.36 ± 1.06	4.59 ± 0.82
Illite	10.25 ± 1.48	9.38 ± 1.91	30.67 ± 4.49	26.18 ± 4.37
Kaolinite	2.40 ± 0.31	6.61 ± 0.84	6.52 ± 1.19	5.82 ± 1.06
Muscovite	1.64 ± 0.23	2.53 ± 0.48	3.54 ± 0.65	3.08 ± 0.64
Orthoclase	1.41 ± 0.21	2.70 ± 0.46	2.06 ± 0.30	2.29 ± 0.40
Anorthite	3.44 ± 0.60	7.29 ± 1.76	9.42 ± 1.88	9.85 ± 2.03
Albite	4.85 ± 0.65	4.17 ± 0.70	9.26 ± 1.37	10.04 ± 1.57
Quartz	15.30 ± 1.69	16.04 ± 5.04	27.36 ± 3.28	32.11 ± 4.98

tillage, which leads to changes in their structural arrangement that affect the total porosity and pore structure. Along with soil erosion, the fine particles are carried away by water flow, while coarser particles are left *in situ*, and some of the finer material becomes the cementing material for microaggregates. The structure of microaggregates reflects, to some extent, the changes in the soil erosion process in the study area.

SEM-EDS planimetric analysis shows that phosphorus (P) was more homogeneous than C in microaggregates from the distribution area (Figures 4, 9). P is a key element for life (Elser et al., 2007), and changes in its composition in soils are closely related to soil and vegetation development. With soil development, the adsorption capacity of clay mineral surfaces for P increases (Reynolds and Davies, 2001). Areas with a high distribution of C are generally lower in Ca (Figure 5). Studies have shown that aggregates are the product of multi-level agglomeration and that SOC is an important cementing substance for the formation of aggregates (Six et al., 2004). Microaggregates are sites of soil carbon sequestration and are important for both C sequestration and soil fertility. The early soil-forming process mainly involves the adsorption of organic matter onto mineral surfaces (Lehmann and Kleber, 2015), which often have chemically reactive properties. Although SOC indirectly affects the soil structure through carbonate, the increase in SOC will lead to the decomposition of carbonate in soil (Bronick and Lal, 2005) (Figure 5). Studies have shown that large aggregates contain less SOC than microaggregates and that SOC may be prevented from being further decomposed through reactions with mineral surfaces and binding to microaggregates (Lehmann and Kleber, 2015). The physical protection of SOC by aggregates is an important mechanism affecting SOC stability. Agglomerate voids also serve as habitats for soil microorganisms. Over time, microorganisms and their mucilage attach to clay particles, forming microaggregates and slowing their biodegradation. Future challenges in soil structure

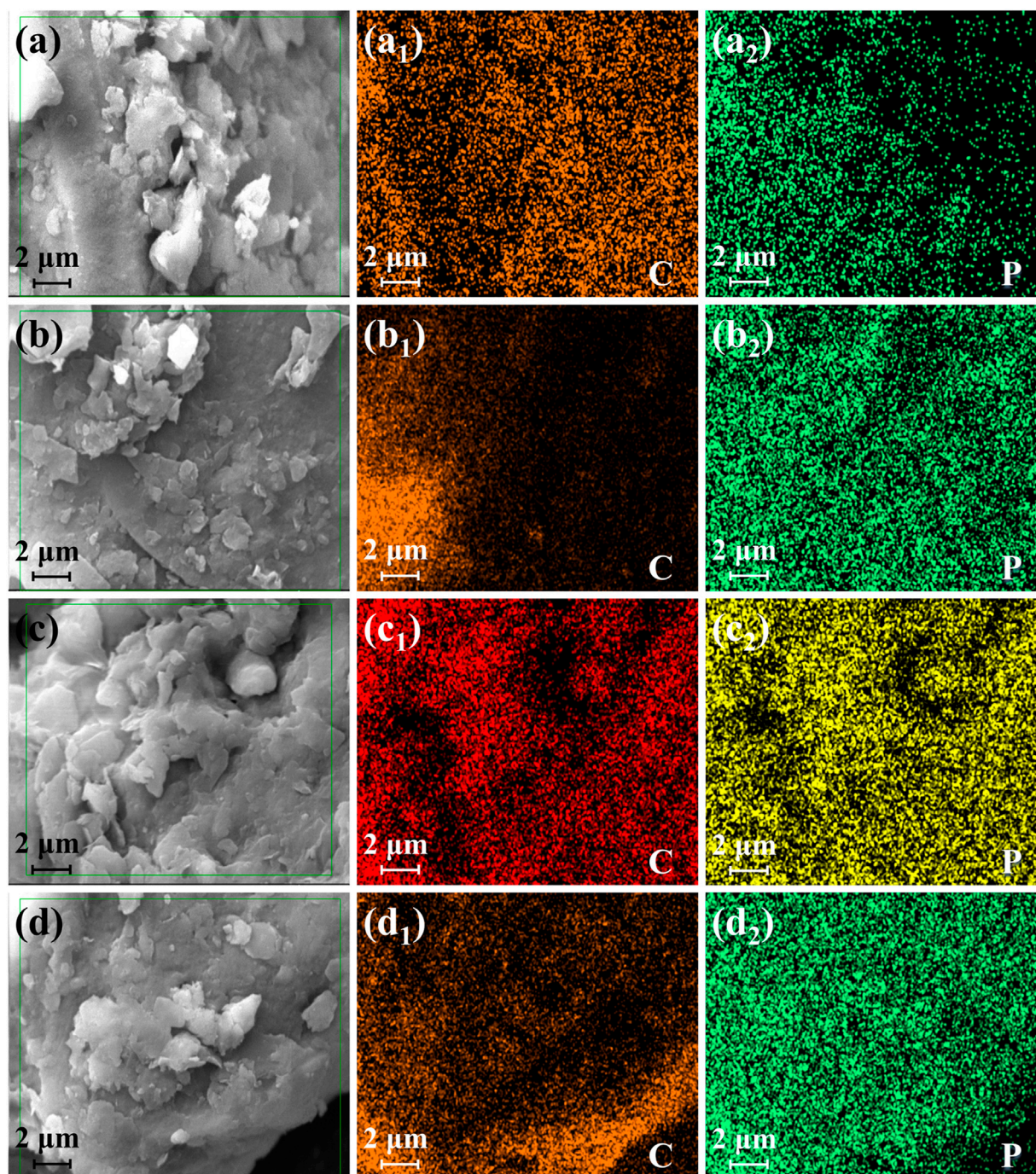
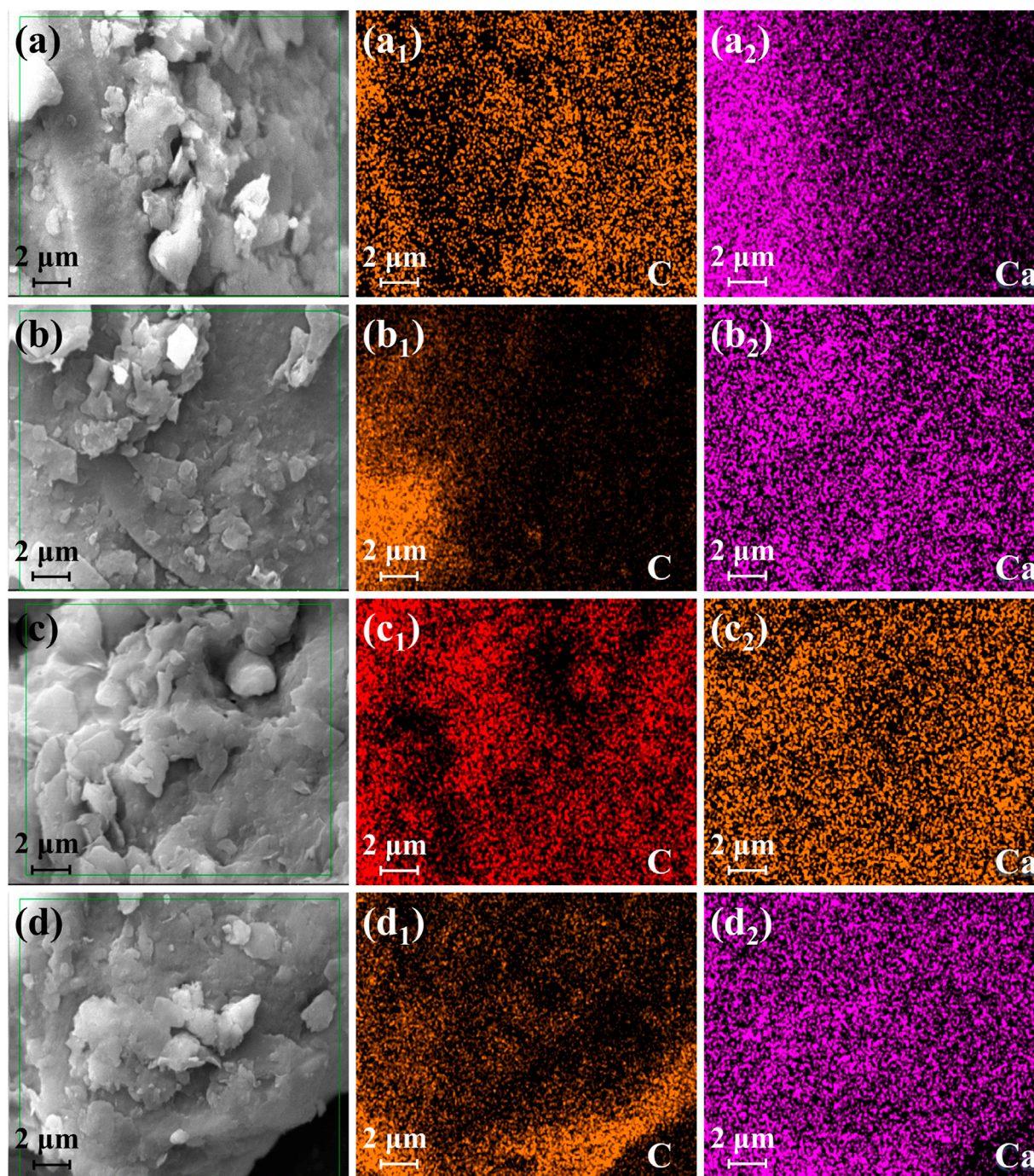


FIGURE 4  
(a<sub>1</sub>–d<sub>1</sub>) represent C in (A–D), respectively; (a<sub>2</sub>–d<sub>2</sub>) represent P in (A–D), respectively.

studies lie in determining the structure of soils, detecting and quantifying microorganisms, and locating active microorganisms at the microscale and nanoscale. The areas of Mg and Al in the microaggregates are mainly distributed on the surfaces of clay particles (Figure 6). Compared to P, Ca is more homogeneous in the microaggregate distribution area (Figure 7), which is related to the high content of limestone minerals, such as calcite and dolomite, in microaggregates in the study area (Table 1). Carbonate

minerals and clay particles are important inorganic cementing agents in microaggregates (Bronick and Lal, 2005). Ca can improve the overall physical, physicochemical, and water properties of soils. The dissolution of carbonate minerals may lead to greater Ca<sup>2+</sup> adsorption on the surfaces of soil colloids, forming a looser microaggregate structure (Figure 2A) (Wang et al., 2011). The elements Mg, Al, and Fe are mainly distributed on the surfaces



**FIGURE 5**  
 (a<sub>1</sub>–d<sub>1</sub>) represent C in (A–D), respectively; (a<sub>2</sub>–d<sub>2</sub>) represent Ca in (A–D), respectively.

of clay particles within microaggregates (Figures 6, 8). The smaller the diameter of the clay particles, the higher the relative cation exchange capacity and the higher the corresponding adsorption capacity of iron ions. The polymeric compounds formed by Al and Fe also have, to some extent, a colloidal flocculating effect on clay colloids.

Studies have shown that variations in the ratios of Al and Fe are related to the ultrastructure of the aggregates (Figures 2, 9) (Calero et al., 2009). The distribution of elements in soils is governed by the distribution of aggregates at different grain levels, and there is a tendency for them to preferentially enrich in clay particles (Acosta et al., 2011; Huang et al., 2017).

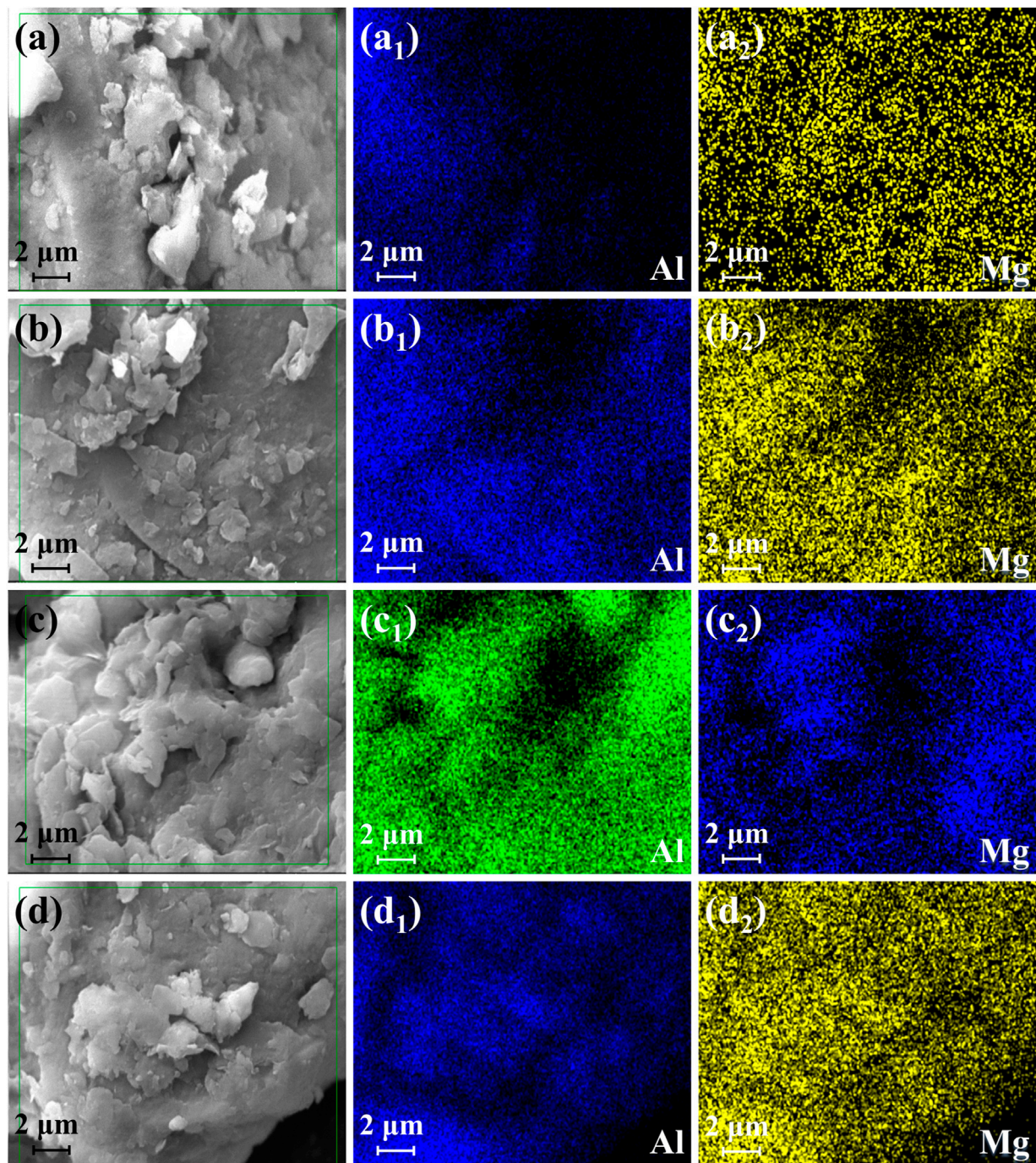
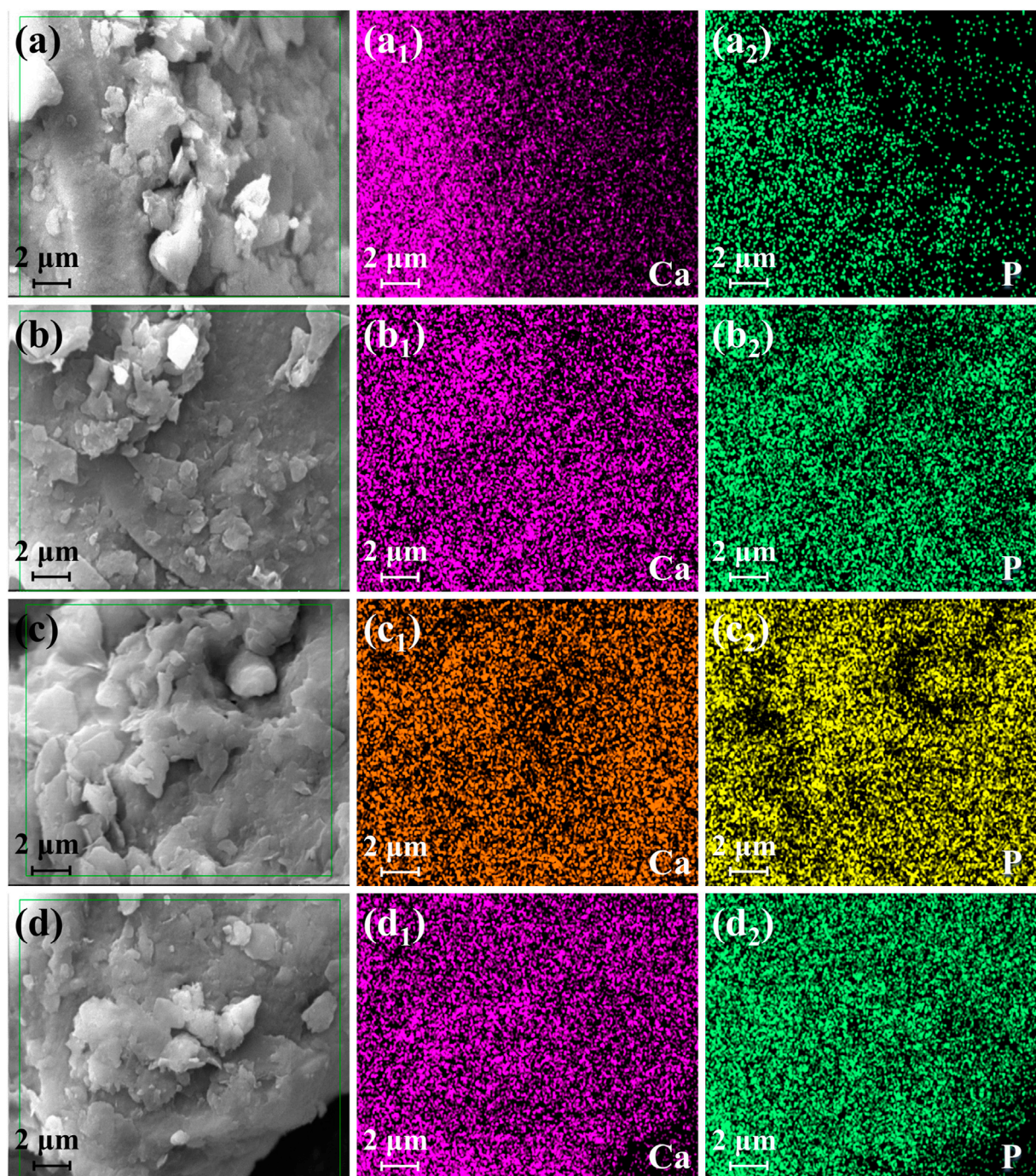


FIGURE 6  
(a<sub>1</sub>–d<sub>1</sub>) represent Al in (A–D), respectively; (a<sub>2</sub>–d<sub>2</sub>) represent Mg in (A–D), respectively.

### 3.2 Mineralogy of soils under different land use types

The XRD analysis revealed that the aggregates contained minerals such as dolomite, calcite, chlorite, illite, kaolinite, muscovite, orthoclase, anorthite, albite, and quartz. The highest contents of dolomite were found in forests and shrublands at 57.1% and 44.41%, respectively, while the lowest were observed in terraces

and cultivated land with 3.70% and 4.84%, respectively. Shrublands had the highest proportion of calcite at 4.14%. The dolomite and calcite content of forests and shrublands is consistent with the local karst geological formation. Long-term cultivation has led to a greater loss in these minerals on terraces and cultivated land. Chlorite had the highest proportion (6.36%) in terraces, indicating the development of yellow-brown soil, which is typical for the region. Illite was present in lower amounts in forests and



**FIGURE 7**  
 (a<sub>1</sub>–d<sub>1</sub>) represent Ca in (A–D), respectively; (a<sub>2</sub>–d<sub>2</sub>) represent P in (A–D), respectively.

shrublands (10.25% and 9.38%, respectively), whereas higher amounts were found in terraces and cultivated land (30.67% and 26.18) (Table 1). Kaolinite content in forest was relatively low at 2.40%, while kaolinite content in shrubland, terraces, and cultivated land was similar. Muscovite increased in forests, shrublands, and terraces while decreasing slightly to 3.08% in cultivated land (Figure 10). Orthoclase had a low content of 1.41% in forests and similar contents in shrublands, terraces, and cultivated land.

Anorthite content decreased in the order of forests, shrublands, terraces, and cultivated land. Albite contents in forests and shrublands were 4.85% and 4.17%, respectively.

The evolution of soil mineralogical composition and elements involves a complex feedback system of geochemical and geomorphic processes within and at the boundaries of the soils (Mavris et al., 2012). The mineralogical composition of the soils in the study area was dominated by dolomite, quartz, illite, anorthite, and albite,

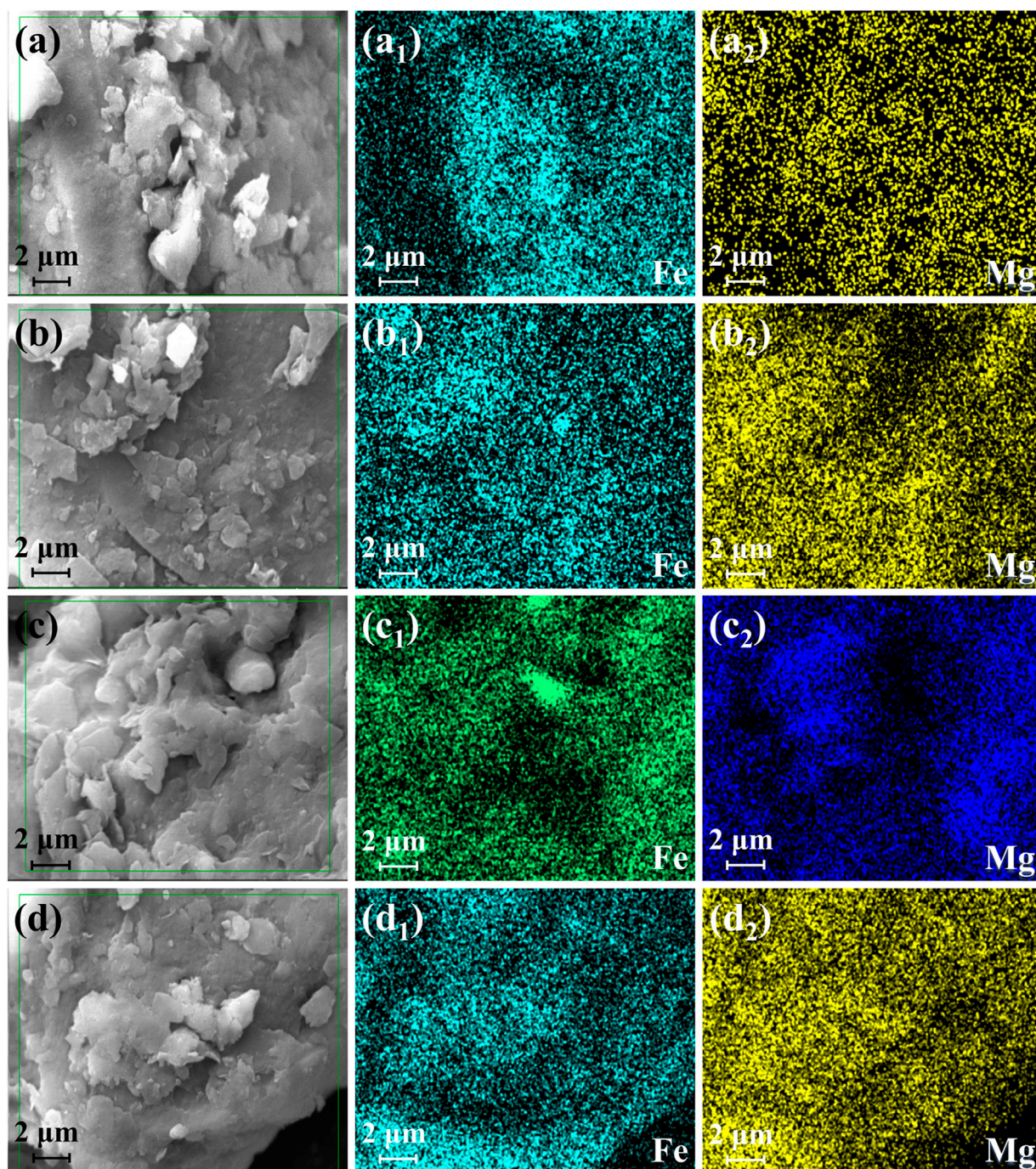


FIGURE 8  
(a<sub>1</sub>–d<sub>1</sub>) represent Fe in (A–D), respectively; (a<sub>2</sub>–d<sub>2</sub>) represent Mg in (A–D), respectively.

which is consistent with the karstic geological background of the area. The main minerals in forest were dolomite, quartz, and illite; in shrubland, there were dolomite, quartz, and illite; in terraces, there were illite, quartz, anorthite, and albite; and in cultivated land, there were quartz, illite, albite, and anorthite (Figure 10; Table 1). The compositions and proportions of illite, chlorite, anorthite, albite, and quartz increased compared with forests and shrublands significantly in terraces and cultivated land (Table 1). The soil mineral assemblage and

crystallinity can indicate the soil-forming stage to some extent, and the illite content of aggregates shows an increasing trend over years of cultivation (Li et al., 2011). The crystallinity of illite in soil reflects the strength of the weathering of soil minerals (Liu et al., 2017), with higher crystallinity indicating weaker weathering. The weathering and soil formation processes are simultaneous, and chemical weathering of minerals is always present throughout the soil formation process. It includes not only the destruction and decomposition of the original

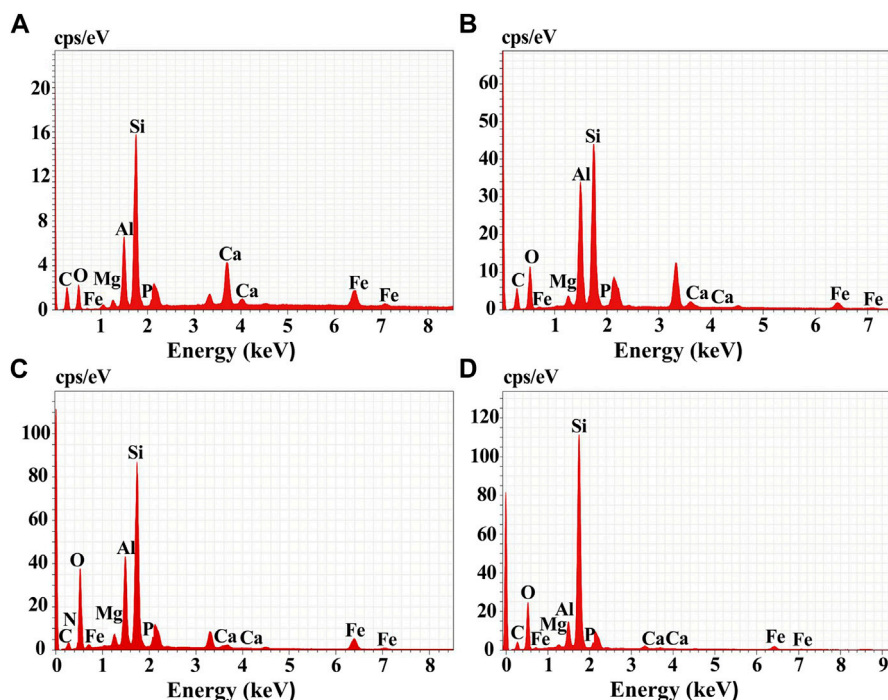


FIGURE 9 SEM-EDS plane scan analysis of the EDS spectrum.

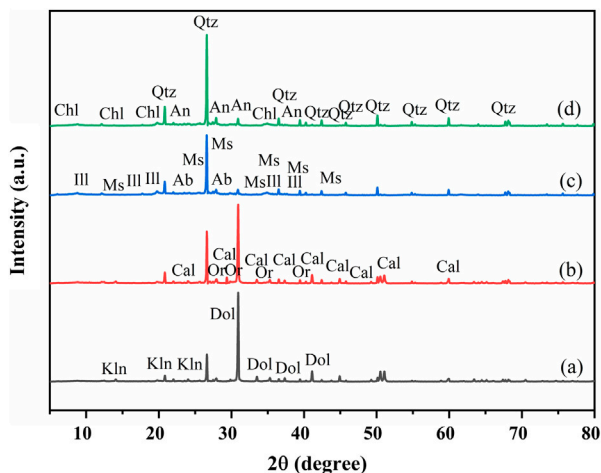


FIGURE 10 X-ray diffractogram patterns (Cu-K $\alpha$  radiation) and mineral change of soil aggregates along the soil chronosequence (Cal, calcite; Chl, chlorite; Dol, dolomite; Ill, illite; Kln, kaolinite; Ms, muscovite; Or, orthoclase; Qtz, quartz; An, anorthite; Ab, albite).

minerals but also the formation of new ones. Owing to long-term weathering and leaching, calcite and dolomite showed gradual decreases over time (Table 1). With weathering of the soil, the leaching of soil minerals, such as calcite and dolomite, occurs. In the early and middle stages of soil weathering, carbonate minerals are

generally dominant (Anderson et al., 2000). Table 1 shows that the content of quartz increased with decreases in altitude because quartz is the most difficult mineral to weather. It is less likely to become a weathering residue during chemical weathering and is therefore enriched and retained in the soil. At the same time, SOC is distributed in soil minerals as discrete particles, where it encases and interacts with soil minerals (Figures 2, 4; Table 1) (Cotrufo et al., 2019; Lavallee et al., 2020; Witzgall et al., 2021). At the clay particle or microaggregate level (<20  $\mu\text{m}$ ), the interactions of clay minerals and SOC with metal oxides dominate (Figures 2, 8; Table 1) (Witzgall et al., 2021).

### 3.3 Biogeochemical cycle under different land use types

Biochemical weathering is the main form of continental surface layer interaction and includes dissolution, leaching, precipitation, and colloid displacement (Yoo and Mudd, 2008). It is also a key link in the elemental geochemical cycle. Aggregates retain SOC, nutrients, and pollutants (Lehmann and Kleber, 2015). Trace elements can have disparate effects on the normal growth of crops, depending on whether they are lacking or in excess. Trace elements are essential for crop growth and development as they can be used by enzymes or coenzymes and are involved in metabolic processes. After entering the soil, trace elements are combined with the surface layer of aggregates through adsorption, complexation, and chelation. Aggregates are important places for the distribution, migration, and transformation of trace elements (Xiao et al., 2016).

TABLE 2 Mass fraction of soil oxides and elements using XRF with standard deviation (mg·Kg<sup>-1</sup>).

Oxide and element	Forest	Shrubland	Terrace	Cultivated land
MgO	56368 ± 17321	55741 ± 17559	21015 ± 12212	16589 ± 12603
Al <sub>2</sub> O <sub>3</sub>	63077 ± 4183	77633 ± 4591	81533 ± 4432	86340 ± 4523
SiO <sub>2</sub>	234881 ± 5169	336540 ± 6197	337540 ± 6010	361347 ± 6215
P <sub>2</sub> O <sub>5</sub>	1688 ± 543	1726 ± 543	656 ± 326	663 ± 309
K <sub>2</sub> O	11452 ± 292	11702 ± 292	14773 ± 311	14174 ± 304
CaO	134262 ± 830	126039 ± 802	21463 ± 344	11702 ± 262
Ti	2834 ± 114	3166 ± 113	3530 ± 106	3625 ± 104
Mn	551 ± 84	587 ± 88	858 ± 94	694 ± 87
Fe	23369 ± 389	25470 ± 404	32067 ± 398	32875 ± 398
Cu	33 ± 11	34 ± 11	32 ± 10	34 ± 10
Zn	47 ± 9	50 ± 10	52 ± 10	56 ± 10
As	9 ± 5	16 ± 6	13 ± 6	16 ± 6
Rb	50 ± 8	56 ± 8	102 ± 10	98 ± 10
Sr	92 ± 10	84 ± 10	87 ± 11	82 ± 10
Y	13 ± 9	17 ± 9	28 ± 10	31 ± 10
Zr	80 ± 8	105 ± 9	162 ± 10	185 ± 10
Pb	29 ± 24	28 ± 23	26 ± 24	24 ± 22

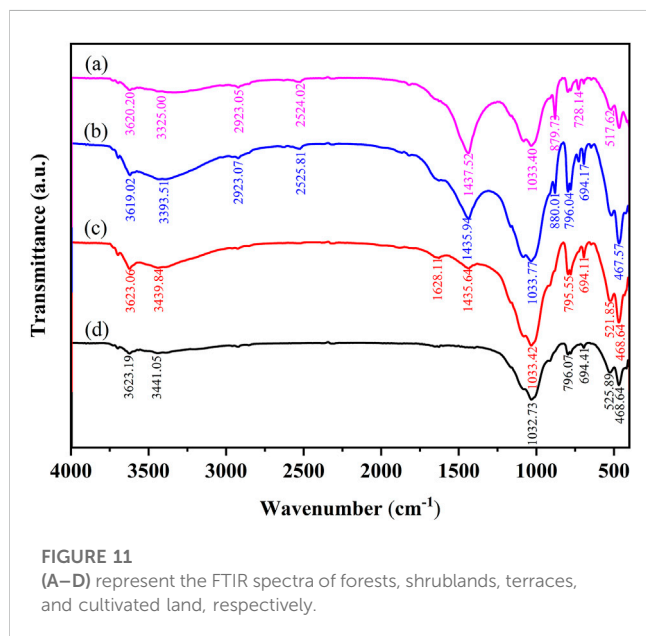


FIGURE 11 (A–D) represent the FTIR spectra of forests, shrublands, terraces, and cultivated land, respectively.

The XRF results show that the contents of Ti, Fe, Zn, Y, and Zr, which are all transitional elements, increased sequentially in forests, shrublands, terraces, and cultivated land (Figure 1; Table 2). The content of Pb in microaggregates decreased in the order of forests, shrublands, terraces, and cultivated land. Rb and Mn had relatively low contents in forests and shrublands and relatively high contents in terraces and cultivated land. There were no significant differences

in the Cu, As, and Sr contents of forests, shrublands, terraces, and cultivated land. Topography is an important influence on soil properties and distributions (Gómez-Plaza et al., 2001; Wongfun et al., 2013). It may have a combined effect on soils according to slope, hydrodynamics, erosion, and deposition (Van Oost et al., 2000). When soils are contaminated with heavy metals, they tend to migrate to water bodies through sink processes and then enter the food chain *via* bioconcentration processes, endangering human health.

SOM is completely mixed with soil minerals and is often attached to them. Meanwhile, SOC usually accounts for <5% of the soil structure (Lehmann and Kleber, 2015). Spectral overlaps often occur between organic matter and minerals. From Figure 11, it can be seen that the intensities of the absorption peaks in the FTIR spectra of aggregates differed according to the land use type. The spectra in forests, shrublands, terraces, and cultivated land all showed a sharp peak at 3,619–3,623 cm<sup>-1</sup>, which is a hydroxyl stretching vibration peak corresponding to clay minerals (Nguyen et al., 1991; Peltre et al., 2014). The change in the integrated area of this peak basically coincides with the change in the contents of clay minerals, such as kaolinite, illite, and chlorite, as shown in Table 1. A broad O-H stretching vibration peak of phenols and alcohols occurred at 3,325–3,441 cm<sup>-1</sup>. The peak at 2,923 cm<sup>-1</sup> is an asymmetric aliphatic CH<sub>2</sub>-stretching vibration peak. The peak at 2,524–2,525 cm<sup>-1</sup> corresponds to the peak for carbonates (Peltre et al., 2014). The peak at 1,628 cm<sup>-1</sup> is composed of clay-bound water (Soriano-Disla et al., 2014). The peak at 1,435–1,437 cm<sup>-1</sup> is for carbonate (Linker et al., 2005; Soriano-Disla et al., 2014; Xing et al., 2019). The peak near 1,032–1,033 cm<sup>-1</sup> is the telescopic vibration of

TABLE 3 Integral of the relative peak area of main peaks of the FTIR spectrum.

$\lambda/\text{cm}^{-1}$	Forest	Shrubland	Terrace	Cultivated land
3619–3623	0.600 ± 0.156	0.658 ± 0.114	0.873 ± 0.121	0.256 ± 0.026
3325–3441	0.588 ± 0.026	0.324 ± 0.110	0.188 ± 0.032	0.137 ± 0.023
2920–2923	0.120 ± 0.010	0.113 ± 0.019	0.073 ± 0.003	0.070 ± 0.004
2524–2525	0.282 ± 0.044	0.325 ± 0.013	0.044 ± 0.004	0.002 ± 0.001
1628–1630	0.028 ± 0.003	0.057 ± 0.012	0.183 ± 0.037	0.032 ± 0.006
1435–1437	27.877 ± 0.702	16.643 ± 0.349	1.778 ± 0.175	0.008 ± 0.002
1032–1033	5.272 ± 0.061	12.757 ± 0.546	11.174 ± 0.298	5.356 ± 0.175
879–880	1.613 ± 0.024	1.139 ± 0.156	0.050 ± 0.009	0.024 ± 0.017

the C–O stretching of polysaccharide or polysaccharide-like material and is also the stretching vibration peak of Si–O in kaolinite (Bernier et al., 2013; Xing et al., 2019). Polysaccharides are thought to be involved in the binding of microaggregates (Cambardella and Elliott, 1994). The peak at 879–880  $\text{cm}^{-1}$  is the out-of-plane bending vibration of the  $\text{CO}_3^{2-}$  group in carbonates (Table 3) (Nguyen et al., 1991; Bernier et al., 2013). The peaks at 1,435–1,437  $\text{cm}^{-1}$  and 870–881  $\text{cm}^{-1}$  are strongly absorbed in relation to carbonate minerals, corroborating the higher calcite and dolomite contents in forests and shrublands, as shown by the quantitative XRD results in Table 1, which is consistent with the local karst geological background. Infrared spectroscopy can provide information on the structure and content of organic functional groups in soils. The results show that the organic fractions and functional groups in forests, shrublands, terraces, and cultivated land were more or less the same, with polysaccharides, phenols, alcohols, and aliphatic substances dominating the organic fractions. The high contents of carbonate minerals in the forests and shrublands are consistent with the karstic geological background of the region. The FTIR results also confirm the fact that the mineral types shown in Table 1 are dominated by silicates, carbonates, clay minerals, and quartz. Gerzabek et al. (2006) found relatively high peaks at 2,920  $\text{cm}^{-1}$ , 1,630  $\text{cm}^{-1}$ , and 1,450  $\text{cm}^{-1}$  in bulk soil and silt-sized fractions, which were correlated with the respective organic C contents. We used the peak integrated areas near the three peaks at 2,920  $\text{cm}^{-1}$ , 1,630  $\text{cm}^{-1}$ , and 1,450  $\text{cm}^{-1}$  to assess the SOM status. Peaks were found in forests and barren slope soils at wave numbers 2,920–2,924  $\text{cm}^{-1}$  but not in soils from terraces and cultivated land. Peaks were found in soils from forests, shrublands, and terraces at 1,627–1,630  $\text{cm}^{-1}$  but not in soils from cultivated land. Peaks were found at 1,435–1,450  $\text{cm}^{-1}$  in soils from forests, shrublands, and terraces but not in soils from cultivated land. The peak area score decreases in the order of forests, shrublands, terraces, and cultivated land (Figure 11; Table 3). It can be concluded that SOM decreases in the order of forests, shrublands, terraces, and cultivated land. The relatively lowest organic matter contents in terraces and cultivated land (especially the latter) may be related to over-tillage. In the early stage of the soil-forming process, it is mainly organic matter that is adsorbed on mineral surfaces, whereas tillage accelerates the decomposition of organic matter (Hidalgo et al., 2019). The intensity of tillage is greater in cultivated land than in terraces. Degradation of aggregates appears to be the main

mechanism for organic matter loss due to long-term tillage (Jastrow, 1996). Indeed, lower numbers of clay particles were attached to the surfaces of microaggregates in terraces and cultivated land, where aggregate degradation may have occurred, than in forests and shrublands (Figures 2, 3). It is recommended that the policy of returning the farmland to forest is strengthened and that economic incentives are explored. There is currently a lack of understanding of the distribution of carbon in aggregates in different land use types in the water source area of the Middle Route of the South-to-North Water Diversion Project. This will be the focus of further research work.

## 4 Conclusion

The structural evolution of microaggregates in different land use types is closely related to biogeochemical processes and alterations of soil mineral assemblages, elements, and organic environments. Microaggregates in forests and shrublands had a flocculent spatial structure, while those in terraces and cultivated land showed plate-like and laminar spatial structures, respectively. The clay mineral composition and carbonate mineral content varied by land use type, with transitional elements showing an enrichment pattern. The organic fraction of the soil mainly consisted of polysaccharides, phenols, alcohols, and aliphatic substances, with cultivated land having relatively low organic matter content, possibly due to over-tillage. The study suggests that returning farmland to forest and exploring complementary economic incentives may be effective measures. The main mechanism of organic matter loss due to long-term tillage appears to be the degradation of microaggregates.

## Data availability statement

The raw data supporting the conclusion of this article will be made available by the authors, without undue reservation.

## Author contributions

Conceptualization, CL; data curation, CL, PQ, and SS; formal analysis, CL; funding acquisition, SG; investigation,

CL; methodology, software, PQ; validation, SS; writing—original draft, CL; and writing—review and editing, CL, SG, and SS. All authors have read and agreed the published version of the manuscript.

## Funding

This work was supported by the Nanyang Normal University scientific research project (grant number: ZX2015088), the Scientific research and service platform fund of Henan Province (grant number: 2016151), and the National Nature Science Foundation of China (grant number: 41601614).

## References

- Acosta, J. A., Martínez-Martínez, S., Faz, A., and Arocena, J. (2011). Accumulations of major and trace elements in particle size fractions of soils on eight different parent materials. *Geoderma* 161, 30–42. doi:10.1016/j.geoderma.2010.12.001
- Anderson, S. P., Drever, J. I., Frost, C. D., and Holden, P. (2000). Chemical weathering in the foreland of a retreating glacier. *Geochim. Cosmochim. Acta* 64, 1173–1189. doi:10.1016/S0016-7037(99)00358-0
- Bernier, M. H., Levy, G. J., Fine, P., and Borisover, M. (2013). Organic matter composition in soils irrigated with treated wastewater: FT-IR spectroscopic analysis of bulk soil samples. *Geoderma* 209–210, 233–240. doi:10.1016/j.geoderma.2013.06.017
- Bronick, C. J., and Lal, R. (2005). Soil structure and management: A review. *Geoderma* 124, 3–22. doi:10.1016/j.geoderma.2004.03.005
- Calero, J., Delgado, R., Delgado, G., and Martín-García, J. M. (2009). SEM image analysis in the study of a soil chronosequence on fluvial terraces of the middle Guadalquivir (southern Spain). *Eur. J. Soil Sci.* 60, 465–480. doi:10.1111/j.1365-2389.2009.01131.x
- Cambardella, C. A., and Elliott, E. T. (1994). Carbon and nitrogen dynamics of soil organic matter fractions from cultivated grassland soils. *Soil Sci. Soc. Am. J.* 58, 123–130. doi:10.2136/sssaj1994.03615995005800010017x
- Cerdà, A. (1996). Soil aggregate stability in three mediterranean environments. *Soil Technol.* 9, 133–140. doi:10.1016/S0933-3630(96)00008-6
- Collins, A. L., Naden, P. S., Sear, D. A., Jones, J. I., Foster, I. D. L., and Morrow, K. (2011). Sediment targets for informing river catchment management: International experience and prospects. *Hydrol. Process.* 25, 2112–2129. doi:10.1002/hyp.7965
- Cotrufo, M. F., Ranalli, M. G., Haddix, M. L., Six, J., and Lugato, E. (2019). Soil carbon storage informed by particulate and mineral-associated organic matter. *Nat. Geosci.* 12, 989–994. doi:10.1038/s41561-019-0484-6
- Duiker, S. W., Rhoton, F. E., Torrent, J., Smeck, N. E., and Lal, R. (2003). Iron (Hydr) Oxide crystallinity effects on soil aggregation. *Soil Sci. Soc. Am. J.* 67, 606–611. doi:10.2136/sssaj2003.6060
- Elser, J. J., Bracken, M. E. S., Cleland, E. E., Gruner, D. S., Harpole, W. S., Hillebrand, H., et al. (2007). Global analysis of nitrogen and phosphorus limitation of primary producers in freshwater, marine and terrestrial ecosystems. *Ecol. Lett.* 10, 1135–1142. doi:10.1111/j.1461-0248.2007.01113.x
- Ersoy, O., Aydar, E., Gourgaud, A., and Bayhan, H. (2008). Quantitative analysis on volcanic ash surfaces: Application of extended depth-of-field (focus) algorithm for light and scanning electron microscopy and 3D reconstruction. *Micron* 39, 128–136. doi:10.1016/j.micron.2006.11.010
- Gerzabek, M. H., Antil, R. S., Kögel-Knabner, I., Knicker, H., Kirchmann, H., and Haberhauer, G. (2006). How are soil use and management reflected by soil organic matter characteristics: A spectroscopic approach. *Eur. J. Soil Sci.* 57, 485–494. doi:10.1111/j.1365-2389.2006.00794.x
- Gómez-Plaza, A., Martí nez-Mena, M., Albaladejo, J., and Castillo, V. M. (2001). Factors regulating spatial distribution of soil water content in small semiarid catchments. *J. Hydrol.* 253, 211–226. doi:10.1016/S0022-1694(01)00483-8
- Haydu-Houdeshell, C.-A., Graham, R. C., Hendrix, P. F., and Peterson, A. C. (2018). Soil aggregate stability under chaparral species in southern California. *Geoderma* 310, 201–208. doi:10.1016/j.geoderma.2017.09.019
- Hidalgo, C., Merino, A., Osorio-Hernández, V., Etchevers, J. D., Figueroa, B., Limon-Ortega, A., et al. (2019). Physical and chemical processes determining soil organic matter dynamics in a managed vertisol in a tropical dryland area. *Soil Tillage Res.* 194, 104348. doi:10.1016/j.still.2019.104348
- Huang, B., Li, Z., Li, D., Yuan, Z., Chen, Z., and Huang, J. (2017). Distribution characteristics of heavy metal(loid)s in aggregates of different size fractions along contaminated paddy soil profile. *Environ. Sci. Pollut. Res.* 24, 23939–23952. doi:10.1007/s11356-017-0012-4
- Igwe, C. A., Zarei, M., and Stahr, K. (2005). Mineral and elemental distribution in soils formed on the River Niger floodplain. *Soil Research* 43 (2), 147–158. doi:10.1071/SR04046
- Jastrow, J. D. (1996). Soil aggregate formation and the accrual of particulate and mineral-associated organic matter. *Soil Biol. Biochem.* 28, 665–676. doi:10.1016/0038-0717(95)00159-X
- Kong, A. Y. Y., Scow, K. M., Córdova-Kreylos, A. L., Holmes, W. E., and Six, J. (2011). Microbial community composition and carbon cycling within soil microenvironments of conventional, low-input, and organic cropping systems. *Soil Biol. Biochem.* 43, 20–30. doi:10.1016/j.soilbio.2010.09.005
- Kuzyakov, Y., and Blagodatskaya, E. (2015). Microbial hotspots and hot moments in soil: Concept and review. *Soil Biol. Biochem.* 83, 184–199. doi:10.1016/j.soilbio.2015.01.025
- Lavallee, J. M., Soong, J. L., and Cotrufo, M. F. (2020). Conceptualizing soil organic matter into particulate and mineral-associated forms to address global change in the 21st century. *Glob. Change Biol.* 26, 261–273. doi:10.1111/gcb.14859
- Lehmann, J., and Kleber, M. (2015). The contentious nature of soil organic matter. *Nature* 528, 60–68. doi:10.1038/nature16069
- Li, C., and Guo, S. (2022). Structural evolution of soil aggregates in a karst rocky desertification area. *RSC Adv.* 12, 21004–21013. doi:10.1039/d2ra02901d
- Li, D. C., Velde, B., Li, F. M., Zhang, G. L., Zhao, M. S., and Huang, L. M. (2011). Impact of long-term alfalfa cropping on soil potassium content and clay minerals in a semi-arid loess Soil in China. *Pedosphere* 21, 522–531. doi:10.1016/S1002-0160(11)60154-9
- Li, L., Zhang, L., Xia, J., Gippel, C. J., Wang, R., and Zeng, S. (2015). Implications of modelled climate and land cover changes on runoff in the middle route of the south to north water transfer project in China. *Water Resour. Manag.* 29, 2563–2579. doi:10.1007/s11269-015-0957-3
- Li, N., Han, L., Zhang, H., Huang, J., Luo, X., Li, X., et al. (2022). Polydopamine nanolayer assisted internal photo-deposition of CdS nanocrystals for stable cosensitized photoanode. *Nano Res.* 15, 8836–8845. doi:10.1007/s12274-022-4588-8
- Linker, R., Shmulevich, I., Kenny, A., and Shaviv, A. (2005). Soil identification and chemometrics for direct determination of nitrate in soils using FTIR-ATR mid-infrared spectroscopy. *Chemosphere* 61, 652–658. doi:10.1016/j.chemosphere.2005.03.034
- Liu, Y. L., Yao, S. H., Han, X. Z., Zhang, B., and Banwart, S. A. (2017). Chapter Six - soil mineralogy changes with different agricultural practices during 8-year soil development from the parent material of a mollisol. *Adv. Agron.* 142, 143–179. doi:10.1016/bs.agron.2016.10.015
- Lu, J., Zheng, F., Li, G., Bian, F., and An, J. (2016). The effects of raindrop impact and runoff detachment on hillslope soil erosion and soil aggregate loss in the Mollisol region of Northeast China. *Soil Tillage Res.* 161, 79–85. doi:10.1016/j.still.2016.04.002
- Margenot, A. J., Calderón, F. J., Bowles, T. M., Parikh, S. J., and Jackson, L. E. (2015). Soil organic matter functional group composition in relation to organic carbon, nitrogen, and phosphorus fractions in organically managed tomato fields. *Soil Sci. Soc. Am. J.* 79, 772–782. doi:10.2136/sssaj2015.02.0070

## Conflict of interest

The authors declare that the research was conducted in the absence of any commercial or financial relationships that could be construed as a potential conflict of interest.

## Publisher's note

All claims expressed in this article are solely those of the authors and do not necessarily represent those of their affiliated organizations, or those of the publisher, the editors, and the reviewers. Any product that may be evaluated in this article, or claim that may be made by its manufacturer, is not guaranteed or endorsed by the publisher.

- Mavris, C., Götze, J., Plötze, M., and Egli, M. (2012). Weathering and mineralogical evolution in a high alpine soil chronosequence: A combined approach using SEM-EDX, cathodoluminescence and nomarski DIC microscopy. *Sediment. Geol.* 280, 108–118. doi:10.1016/j.sedgeo.2012.04.008
- McCrackin, M., Jones, H., Jones, P., and Moreno Mateos, D. (2016). Recovery of lakes and coastal marine ecosystems from eutrophication: A global meta-analysis. *Limnol. Oceanogr.* 62, 507–518. doi:10.1002/lno.10441
- Mganga, K. Z., Razavi, B. S., and Kuzyakov, Y. (2016). Land use affects soil biochemical properties in Mt. Kilimanjaro region. *CATENA* 141, 22–29. doi:10.1016/j.catena.2016.02.013
- Nguyen, T. T. D., Janik, L. J., and Raupach, M. (1991). Diffuse reflectance infrared Fourier transform (DRIFT) spectroscopy in soil studies. *Soil Res.* 29, 49–67. doi:10.1071/SR9910049
- Oades, J. M., and Waters, A. G. (1991). Aggregate hierarchy in soils. *Soil Res.* 29, 815–828. doi:10.1071/SR9910815
- Parent, L. C., de Almeida, C. X., Hernandes, A., Egozcue, J. J., Gülsler, C., and Bolinder, M. A. (2012). Compositional analysis for an unbiased measure of soil aggregation. *Geoderma* 179, 123–131. doi:10.1016/j.geoderma.2012.02.022
- Peltre, C., Bruun, S., Du, C., Thomsen, I. K., and Jensen, L. S. (2014). Assessing soil constituents and labile soil organic carbon by mid-infrared photoacoustic spectroscopy. *Soil Biol. Biochem.* 77, 41–50. doi:10.1016/j.soilbio.2014.06.022
- Pronk, G. J., Heister, K., Ding, G.-C., Smalla, K., and Kögel-Knabner, I. (2012). Development of biogeochemical interfaces in an artificial soil incubation experiment; aggregation and formation of organo-mineral associations. *Geoderma* 189–190, 585–594. doi:10.1016/j.geoderma.2012.05.020
- Rabot, E., Wiesmeier, M., Schlüter, S., and Vogel, H. J. (2018). Soil structure as an indicator of soil functions: A review. *Geoderma* 314, 122–137. doi:10.1016/j.geoderma.2017.11.009
- Reynolds, C. S., and Davies, P. S. (2001). Sources and bioavailability of phosphorus fractions in freshwaters: A British perspective. *Biol. Rev. Camb. Philos. Soc.* 76, 27–64. doi:10.1017/s1464793100005625
- Sander, T., Gerke, H. H., and Rogasik, H. (2008). Assessment of Chinese paddy-soil structure using X-ray computed tomography. *Geoderma* 145, 303–314. doi:10.1016/j.geoderma.2008.03.024
- Six, J., Bossuyt, H., Degryze, S., and Deneef, K. (2004). A history of research on the link between (micro)aggregates, soil biota, and soil organic matter dynamics. *Soil Tillage Res.* 79, 7–31. doi:10.1016/j.still.2004.03.008
- Soriano-Disla, J. M., Janik, L. J., Viscarra Rossel, R. A., Macdonald, L. M., and McLaughlin, M. J. (2014). The Performance of Visible, near-and mid-infrared reflectance spectroscopy for prediction of soil physical, chemical, and biological properties. *Appl. Spectrosc. Rev.* 49, 139–186. doi:10.1080/05704928.2013.811081
- Tang, Q., Peng, L., Yang, Y., Lin, Q., Qian, S. S., and Han, B.-P. (2019). Total phosphorus-precipitation and Chlorophyll a-phosphorus relationships of lakes and reservoirs mediated by soil iron at regional scale. *Water Res.* 154, 136–143. doi:10.1016/j.watres.2019.01.038
- Van Oost, K., Govers, G., and Desmet, P. (2000). Evaluating the effects of changes in landscape structure on soil erosion by water and tillage. *Landsc. Ecol.* 15, 577–589. doi:10.1023/A:1008198215674
- Wang, W. J., He, H. S., Zu, Y. G., Guan, Y., Liu, Z. G., Zhang, Z. H., et al. (2011). Addition of HPMA affects seed germination, plant growth and properties of heavy saline-alkali soil in northeastern China: Comparison with other agents and determination of the mechanism. *Plant Soil* 339, 177–191. doi:10.1007/s11104-010-0565-1
- Witzgall, K., Vidal, A., Schubert, D. I., Höschen, C., Schweizer, S. A., Buegger, F., et al. (2021). Particulate organic matter as a functional soil component for persistent soil organic carbon. *Nat. Commun.* 12, 4115. doi:10.1038/s41467-021-24192-8
- Wongfun, N., Götze, J., Furrer, G., Brandl, H., and Plötze, M. (2013). Effect of water regime and vegetation on initial granite weathering in a glacier forefield: Evidences from CL, SEM, and Nomarski DIC microscopy. *Geoderma* 211–212, 116–127. doi:10.1016/j.geoderma.2013.07.009
- Xiao, R., Zhang, M., Yao, X., Ma, Z., Yu, F., and Bai, J. (2016). Heavy metal distribution in different soil aggregate size classes from restored brackish marsh, oil exploitation zone, and tidal mud flat of the Yellow River Delta. *J. Soils Sediments* 16, 821–830. doi:10.1007/s11368-015-1274-4
- Xing, Z., Tian, K., Du, C., Li, C., Zhou, J., and Chen, Z. (2019). Agricultural soil characterization by FTIR spectroscopy at micrometer scales: Depth profiling by photoacoustic spectroscopy. *Geoderma* 335, 94–103. doi:10.1016/j.geoderma.2018.08.003
- Yoo, K., and Mudd, S. M. (2008). Toward process-based modeling of geochemical soil formation across diverse landforms: A new mathematical framework. *Geoderma* 146, 248–260. doi:10.1016/j.geoderma.2008.05.029